SCIENCE CHINA
Information Sciences

• RESEARCH PAPER •

October 2019, Vol. 62 202402:1–202402:11
https://doi.org/10.1007/s11432-019-9906-1

A flexible skin-mounted wireless acoustic device for bowel sounds monitoring and evaluation

Fengle WANG[1], Dong WU[2], Peng JIN[1], Yingchao ZHANG[1], Yingyun YANG[2], Yinji MA[1], Aiming YANG[2], Ji FU[1*] & Xue FENG[1*]

[1]*Key Laboratory of Applied Mechanics, Department of Engineering Mechanics, Tsinghua University, Beijing* 100084*, China;*
[2]*Department of Gastroenterology, Peking Union Medical College Hospital, Beijing* 100730*, China*

Received 18 March 2019/Revised 14 May 2019/Accepted 23 May 2019/Published online 2 September 2019

Abstract Conventional methods of intestinal inspection play an essential role in the assessment of bowel diseases and other relevant health issues, yet fail to obtain intestinal conditions in real time because of radiation limits and operation inconvenience. Herein, a flexible, skin-mounted device is developed for long-term, real-time monitoring, and for the evaluation of bowel sounds based on the integration of a three-dimensional printed elastomeric resonator with flexible electronics. The device is capable of being flexibly attached to abdominal surfaces without performance degradation during breathing. Clinical tests conduct in a normal volunteer and in patients with mechanical intestinal obstruction or paralytic ileus illustrate the usefulness of the device in capturing the characteristics of bowel sounds. Furthermore, a demonstration of collection and classification of bowel sounds by the flexible device based on machine learning methods can serve as a reference for possible applications of the system in the auxiliary diagnosis of bowel problems.

Keywords flexible wearable device, bowel sounds, long-term monitoring, machine learning, intestinal motility

Citation Wang F L, Wu D, Jin P, et al. A flexible skin-mounted wireless acoustic device for bowel sounds monitoring and evaluation. Sci China Inf Sci, 2019, 62(10): 202402, https://doi.org/10.1007/s11432-019-9906-1

1 Introduction

Patients suffering from bowel disease, such as colon cancer and irritable bowel syndrome, or medical and neurological diseases that partly involve the intestinal tract, usually suffer from motility and functional bowel disorders [1–3]. Effective assessment of the patient intestinal conditions plays a vital role in the diagnosis and evaluation of these diseases [4, 5]. Unfortunately, the conventional techniques presently used are time-consuming and patient-unfriendly, and most of them even need expensive and cumbersome instruments, such as enteroscopy, abdominal fluoroscopy, computed tomography, and abdominal sonography. Moreover, X-ray-based techniques are limited owing to the duration and frequency of the radiologic procedures [6]. Auscultation of physiological sounds exists as a simple but classical and extensively employed method for medical investigation, especially for cardiac and pulmonary sounds. Similarly, bowel sounds generated from the movement of the intestinal contents and gas during peristalsis, are recognized clinically as useful indicators of intestinal function [7–10]. For example, hyperactive bowel sounds ("loud", "high-pitched" and "tinkling" sounds) may be the result of diarrhea or early intestinal obstruction while hypoactive bowel sounds (very diminished or absent sounds) are correlated with bowel obstruction, paralytic ileus, torsion of the bowel, or peritonitis, and can cause diminished peristalsis [11, 12]. Therefore,

* Corresponding author (email: fuji@cheroee.com, fengxue@tsinghua.edu.cn)

although endoscopic or imaging examinations possess the capacity and accuracy for diseases diagnoses, auscultation of bowel sounds can serve as the primary diagnostic approach owing to its low cost and minimal pain according to current clinical practice. Additionally, it has great potential for utilization according to several studies and for setting criteria for the disease diagnoses, such as irritable bowel syndrome [9, 13], Crohn's disease [13], intestinal obstruction [14], and acute abdominal diseases [15].

Additionally, a reliable and valuable way of diagnosis based on bowel sounds is the possible combination of long-term continuous monitoring of these sounds with appropriate signal analyses. This is attributed to the fact that bowel sounds may appear at irregular time intervals [8]. For example, bowel sounds may not exist for several hours in the intestinal tract of patients with postoperative ileus. They are also affected by various factors, including intestinal motility, medication, and intestinal content [16–18]. However, existing commercial electronic stethoscopes with hard, bulky acoustic resonators and stiff circuit boards, prevent them from being wearable, portable, or conformal with curved body surfaces [8,9,19–21]. In recent years, wireless wearable devices have become a promising trend in the field of medical care and diagnosis owing to the advantages of long-term continuous health monitoring and remote consultation [22–26]. However, wearable acoustic devices used for the detection of bowel sounds rely on a satisfactory interface of the device with the curvilinear parts of the human body surface [27], and on specifically developed signal analysis methods, including filtering, feature extraction and classification.

This study presents a flexible and wearable wireless system that aims to conduct the long-term, real-time monitoring and analyses of vital sound signals within the intestinal tract (Figure 1(a)). The device is attached to the curved abdominal surface. Qualitative improvements in its flexibility and wearability are achieved following implementation of a flat three-dimensional (3D) printed elastomeric resonator and a tiny microelectromechanical systems (MEMS) microphone positioned on the flexible substrate. By means of a low-power Bluetooth chip, the bowel sound signals can be transmitted to a mobile handset for the waveform display and data storage. Experimental tests of bowel sound recording during digestion verify its validity of long-term continuous monitoring of intestinal motility, while clinical tests show that it can capture the characteristics of bowel sounds between the normal subject and patients with mechanical intestinal obstruction (MIO) or paralytic ileus. Furthermore, we demonstrate the use of the flexible device for the collection and classification of bowel sounds produced separately in the digestion of nuts and oranges, by using back-propagation neural networks (BPNN). Based on the reported average recognition accuracy of the 10-fold cross-validation of 76.89%, the system has the potential to be a complementary tool for continuous and noninvasive evaluation of intestinal conditions (Figure 1(b)).

2 Results and discussion

2.1 Device design and resonator considerations

This device incorporates a specifically designed sound collection structure, that is, the 3D printed elastomeric resonator (41.9 mm×30.2 mm×7.8 mm, Young's modulus: ∼0.3 MPa) and a small MEMS microphone chip, at one end of the flexible polyimide (PI) board (Figure 1(c)). The resonator has a flat U shape (height: 7.8 mm) with two cavities of different cross-sectional areas. The PI board contains a low-power Bluetooth chip for signal transmission and other electronic components. The location of the microphone chip is separated from the area where the main circuit components reside to reinforce the flexible board's reliability in repetitive bending conditions (Figure 1(d)). An ultra-soft thin layer of biocompatible silicone serves as the shell (thickness: ∼2 mm). The power supply is supported by a small rechargeable battery that can be bent (Figure 1(e)). Sound waveforms can be displayed by a custom-developed mobile application in real time, and the data can be stored in the mobile phone (Figure 1(f)). The result is a lightweight flexible device (with an approximate weight of 6.5 g) that can accommodate large deformations as shown in Figure 1(g). When the device is attached to the abdominal surface, it can bend as the stomach rises and falls during respiration without any functional failure. Additionally, it does not cause any discomfort to the subjects (Figure 1(h)).

It is essential for the 3D printed resonator and the microphone to provide good physiological acoustic

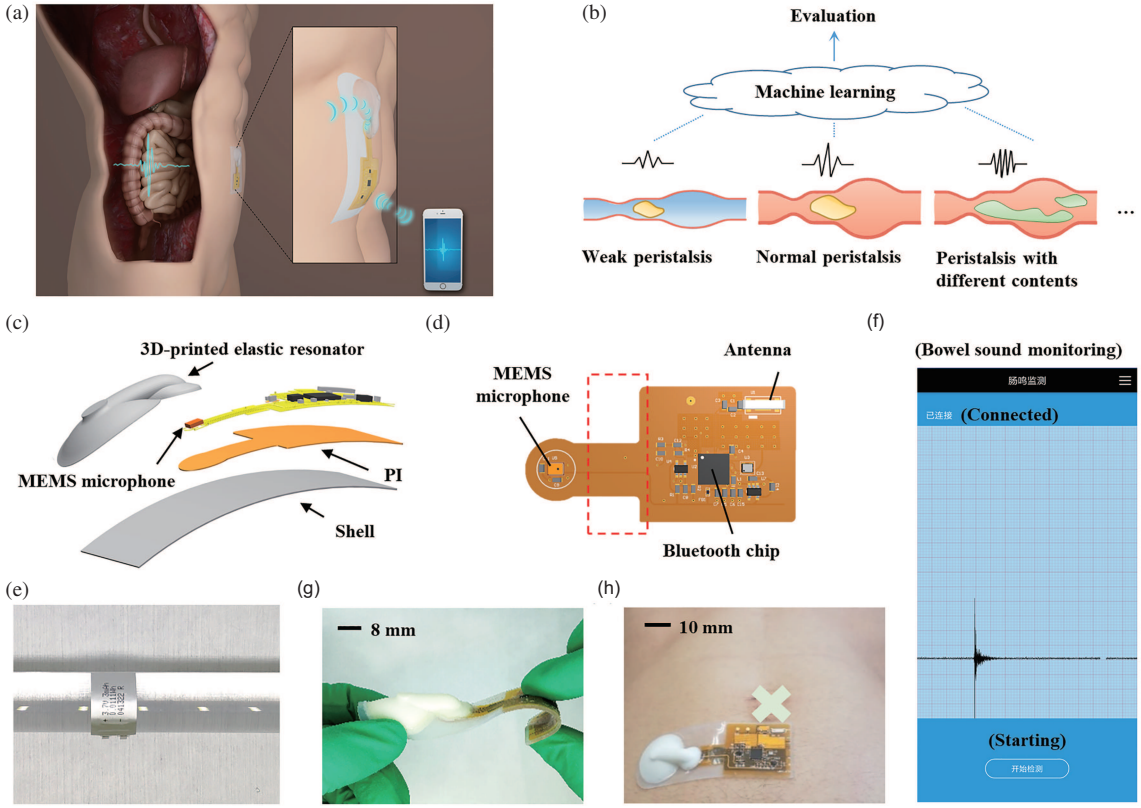

Figure 1 (Color online) Working principle and design of the flexible acoustic device. (a) Schematic of the flexible skin-mounted wireless acoustic device for bowel sound detection. (b) Illustration of the principle of the device for evaluations of bowel problems, based on a machine learning model of different intestinal conditions, such as weak peristalsis, or peristalsis with poisonous contents. (c) Exploded view diagram of the overall design structure of the device. (d) Layout of device's circuit. The red dotted rectangle separates MEMS microphone chip and the main circuit component area to reinforce the flexible board's bending performance. (e) Small rechargeable battery that can be bent on a rod with a diameter of 2 cm. (f) Waveform display in mobile application. (g) Bent device using the fingers. (h) Device mounted on the curved abdominal surface.

sensing without losing portability. To be well sensed by the microphone, bowel sounds arriving at the abdominal surface first enter from the large cavity of the resonator, and then pass through a flat channel, and they are finally collected into the other small cavity (Figure 2(a)). The radius of the middle channel, wall thickness, and shell thickness are the main variables considered in the design of the resonator. Other factors, like the inlet and outlet diameters of cavities, are restricted by the device size, and the channel length should be the minimized because sound energy dissipates more with longer channels. Herein, the device has a channel length l of 15.5 mm, an inlet diameter of 21.87 mm, and an outlet diameter of 9.04 mm.

The channel section can be ideally modeled as a short slim pipe (Figure 2(b)) whose length l and radius a are much smaller than the bowel sound wavelength (0.34–6.8 m) [7, 8, 10, 28]. When there is a wave with the velocity v, the acoustic resistance R_a is given by [29]

$$R_a = \frac{l}{\pi a^3}\sqrt{2\eta\omega\rho_0}, \tag{1}$$

where ω is the sound frequency, and ρ_0 and η denote the medium density and coefficient of shear viscosity respectively. As the medium is air, ρ_0 and η are respectively set to 1.29 kg/m^3 and 1.983×10^{-5} Pa·s. Figure 2(c) illustrates the relationship between R_a and a for three sound waves at the frequencies of 50, 150 and 1000 Hz. This shows that as a ranges from 1 to 2 mm, R_a declines by approximately 87.5%. Herein, a is chosen to be equal to 2 mm in consideration of the device size.

Usually there is a compromise between the maximized sound insulation and the desirable small and flexible acoustical device. To find a reasonable wall thickness, another existing method is used to study

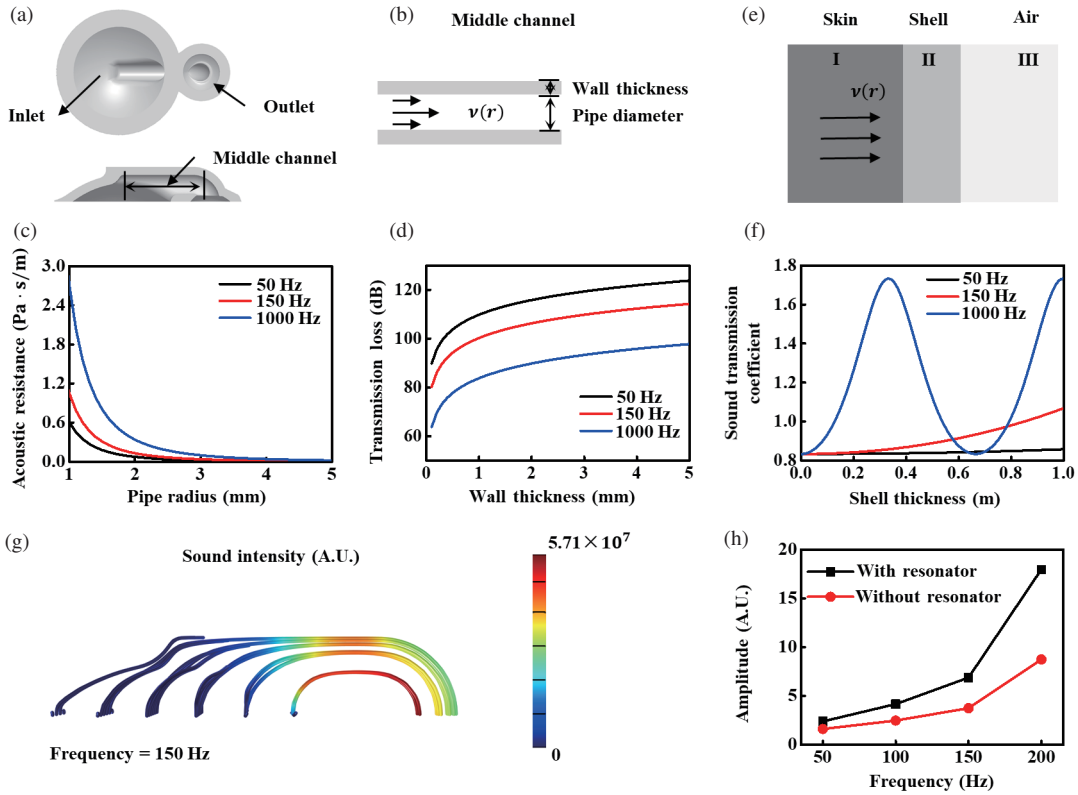

Figure 2 (Color online) Design of resonator. (a) Top and cross-sectional views of the resonator structure; (b) a pipe model ideally transformed from the channel section of the resonator; (c) curves of acoustic resistance vs. pipe radius and (d) transmission loss vs. wall thickness for sound frequencies of 50, 150 and 1000 Hz; (e) a skin-shell-air model depicting the transmission of a sound wave through the shell; (f) sound transmission coefficient vs. shell thickness curves for the sound frequencies of 50, 150 and 1000 Hz; (g) sound intensity streamlines in the resonator in lateral view at the sound frequency of 150 Hz; (h) comparison of the received sound signal amplitude when the device faces the same sounds with and without a resonator.

the effect of a varying wall thickness on the transmission loss TL of the pipe wall. In this research it is assumed that atmospheric air is contained inside and outside the pipe at the same atmospheric pressure. Therefore, TL has the following form [30]:

$$\mathrm{TL} = 10\log_{10}\frac{t^2}{2a^2} + 20\log_{10}\frac{f_0}{f_p} + 66.5, \tag{2}$$

where t is the pipe wall thickness (f_0 and f_p can be found in Appendix B). As Figure 2(d) shows, the TL value of the pipe wall exhibits a gradually weakened rising trend as t increases, which means that the thicker wall has a more effective sound insulation. The increase in TL associated with the wall thicknesses of 0.1 and 2 mm is approximately 25 dB for sound frequencies in the range of 50 to 1000 Hz. At same wall thickness, the pipe wall allows larger transmission losses for lower sound frequencies, so the pipe model acts like a lowpass filter. However, because of size limits t is finally determined to be equal to 2 mm.

The simple skin-shell-air model (Figure 2(e)) predicts the transmission of a sound wave at different thicknesses of the shell layer. It is assumed that the incident, reflected and transmitted bowel sound waves, can be regarded to be planar, and both interfaces between the three media are flat. The sound transmission coefficient t_I is defined as the intensity ratio of the incident wave to the transmitted wave. This coeffient has been defiend from a previous analysis of normally incident sound and its transmission through a single-leaf partition [31], and it is given by

$$t_I = \frac{R_1}{R_3}\frac{8}{[(\frac{R_1}{R_2}+\frac{R_2}{R_3})^2+(1+\frac{R_1}{R_3})^2]-[(\frac{R_1}{R_2}+\frac{R_2}{R_3})^2-(1+\frac{R_1}{R_3})^2]\cos\frac{2\pi}{\lambda_2}D}, \tag{3}$$

where λ_2 is the sound wavelength and D is the thickness of the shell layer. R_1, R_2, and R_3 refer to acoustic resistances of the skin, shell layer, and air respectively. From this equation, t_I reaches the maximum when D is equal to $\lambda_2/4$. Figure 2(f) shows the variation trend of t_I as a function of D at the sound frequencies of 50, 150, and 1000 Hz ($R_1 = 1.99\times10^6$ Pa·s/m, $R_2 = 1.38\times10^6$ Pa·s/m and $R_3 =$ 415 Pa·s/m). However, D should be much less than the size of a quarter of the bowel sound wavelength (approximately equal to several hundred millimeters) to make our device thin and light. In this range, the sound transmission efficiency slightly grows with the layer thickness. Therefore, D is finally chosen to be equal to 5 mm.

Figure 2(g) shows a lateral view of the streamline visualization for presenting finite element analysis (FEA) of the sound intensity field in the resonator, where the transmission of sound waves (frequency = 150 Hz) in this structure lead to a significantly enhanced sound intensity in the outlet. Furthermore, an experiment is conducted to compare the responses of our device to the sound source at a specific distance with and without the resonator. Results indicate that the device integrated with the resonator exhibits increased sound amplitudes in the range of 50–200 Hz, as expected from the amplification effect of sound transmission (Figure 2(h)).

2.2 Device characterization

The raw response of the acoustic device to bowel sounds from a healthy male subject (age = 23 years) is shown in Figure 3(a) in the form of a continuous waveform line, whereby each wave is a sound pulse. The device is placed on the lower abdomen. The sampling rate of our device is fixed at 2000 Hz, and is no less than two times the highest frequency of the bowel sound (at around 1000 Hz). Based on these recordings, there are two clusters of sounds on the left side followed by several isolated sounds. The "isolated" sounds occurr in isolation, and appeare as a vertical line, while the "cluster" of sounds are recognized audibly as a run of individual "popping" effects with longer durations [8, 32]. Figure 3(b) shows a comparison of signals measured simultaneously by a commercial e-stethoscope within an interval of ∼0.1 s. Partly because of the slightly lower signal-to-noise ratio, and partly because of the lower sampling rate, the acoustic signals from our device are not completely consistent compared to those obtained using the commercial e-stethoscope, but all the key features of the two waveforms are highlighted. For example, the relative value of different signal peaks, sound durations and sound-to-sound intervals have a good consistency.

Tests that involve deep abdominal breathing with the device attached on the skin around the navel demonstrate flexibility and reliability (Figure 3(c)). During inhalation (red line) and exhalation (blue line), the device can bear the changes of curvature in the abdominal surface and output the measured sound signals as shown in Figure 3(d). Magnified views of two 0.3 s segments during inhalation (left) and exhalation (right) show consistency in the noise levels during the bending process of the device. This implies the deformation has no effect on the signal. Besides, the approximate maximum bending curvature of the acoustic device is 2.4 m^{-1} (Figure 3(e)).

2.3 Long time recording and evaluation

The special feature of the flexible, skin-mounted acoustic device, that is, its compatibility with direct placement on curvilinear regions of the skin, enable the application in long-term continuous monitoring for bowel sounds. This can reveal the pattern of intestinal activity, type of intaken food, and even the blood glucose levels [28]. Therefore, a nearly five-hour experiment is implemented to monitor changes of bowel sounds of the same healthy male subject after food intake in a silent room. From 13:00 pm to 17:45 pm bowel motility manifest a gradual decline followed by a large sound increase (Figure 4(a)). In Figure 4(b), the variation of the number of peaks and short-time energy over time are shown in the form of a histogram and a broken line graph. The total acquisition period which spann 285 min is divided into 56 segments, and each of them spanned 10 min with a 50% overlap with the successive and preceeding bins. In this way, the number of peaks or short-time energy represents the sum of the peaks or the energy within a period of 10 min, and are plotted at the mid points of the corresponding bins. Only peaks whose

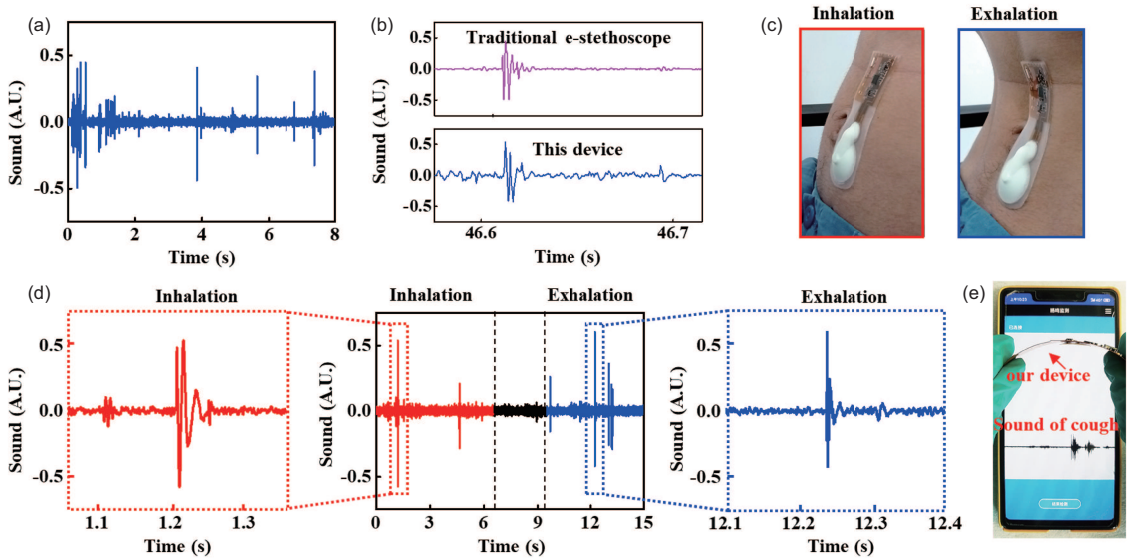

Figure 3 (Color online) Comparison between the flexible acoustic device and commercial e-stethoscope for experimental characterization during abdominal breathing. (a) Example of a recorded bowel sound waveform. Each wave is a bowel sound pulse. (b) Comparison of simultaneous recordings using a commercial e-stethoscope and our device. (c) Photographs of the attached flexible acoustic device during an abdominal respiratory cycle. (d) Plots of measured signals during inhalation and exhalation. In the middle image, the black line between the red line (inhalation) and blue line (exhalation) represents the end-inspiratory pause. Magnified views of the two bowel sounds during inhalation (left) and exhalation (right). (e) The approximate maximum bending curvature of the acoustic device.

value surpass an empirically determined intensity threshold of 0.2 arbitrary units are counted to lower the influence of noise. The short-time energy E_n of segment n is obtained by

$$E_n = \sum_{m=0}^{N-1} x_n^2(m), \tag{4}$$

where N is the number of data in segment n and $x_n(m)$ is one of the data points.

Clearly bowel sounds present locally random but generally regular changes regarding the number of peaks and short-time energy over a prolonged time period. After food intake the activity of bowel sounds is at a relatively high level for more than an hour. This activity is then stabilized before the next meal time whereby another considerable increase is manifested (Figure 4(b)), just like a growling stomach. It is also found that drinking water may have minor influence on the production of bowel sounds. The spectrogram obtained with the use of short-time Fourier transform displays the frequency distribution as a sequence of vertical lines, and the higher power levels of the sound frequencies have darker color tones (Figure 4(c)). It appears that lower frequency components (below 600 Hz) exhibit larger changes. In conclusion, by using the flexible device for long time monitoring, all these characteristics of bowel sounds are shown to experience changes after food intake. These changes could not be detected easily by hard, bulky commercial stethoscopes. Based on the proposed type of examination, information about one's long-term digestive motility can be collected and understood by clinicians.

2.4 Cilinical tests of device

To test the performance of the device in patients, the bowel sounds of one normal subject (male, age of 24 years), one female patient (age of 28 years) with MIO, and another female patient (age of 35 years) with paralytic ileus, were collected in the hosptial. Typical time-domain waveforms are shown in Figure 5(a). The number of peaks in the MIO-trace is the largest (233 peaks) among these three samples, and the smallest in the paralytic ileus traces is smallest (22 peaks). Regarding the power envelope curves in Figure 5(b), they also have different peak values and positions. This implies the existence of differences in the peristaltic bowel sound models. Although these three samples yield a seemingly regular and distinct

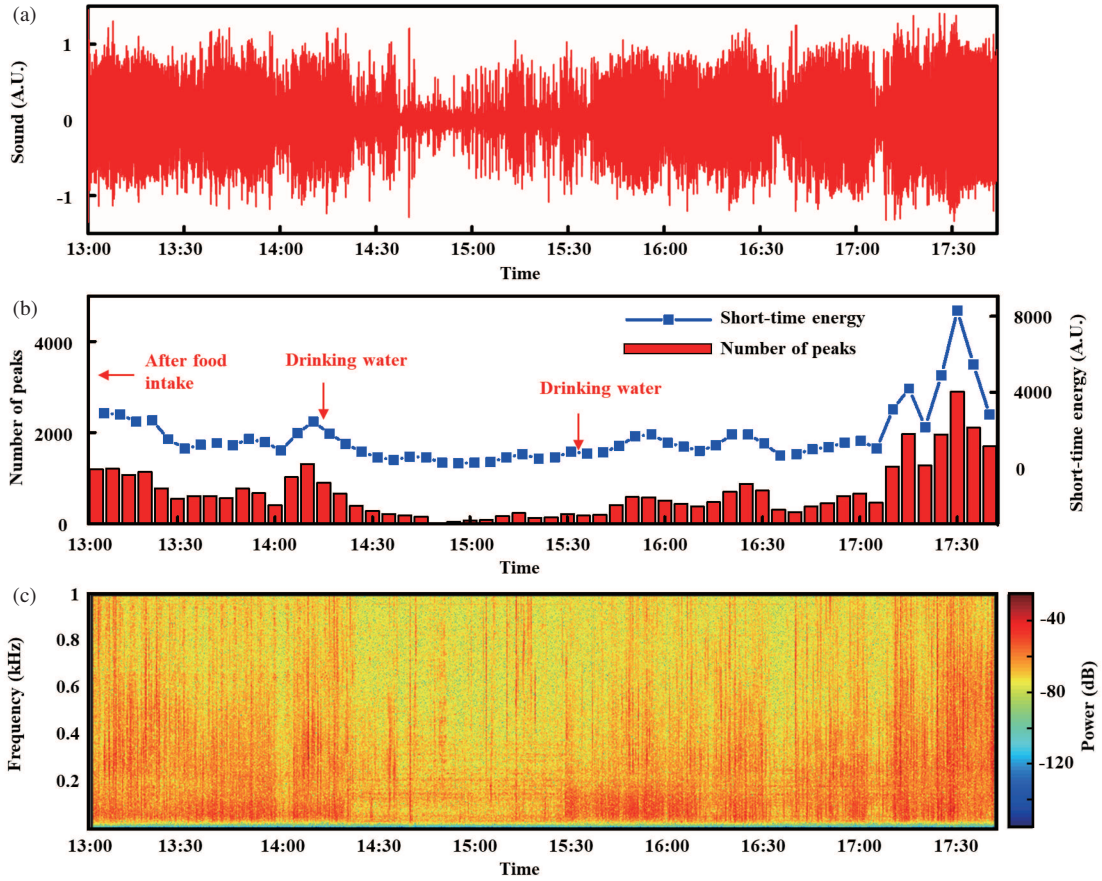

Figure 4 (Color online) Long time evaluation of bowel sounds. (a) Bowel sound variations for near five hours after food intake; (b) variation of number of peaks (in histogram) and short-time energy (broken line) of bowel sounds over time; (c) spectrogram of bowel sounds (darker color means higher spectral power along the y-axis) using short-time Fourier transform.

comparison, it is necessary to mention that there are large amplitude variations of the waveform in both the time and frequency domains for each of these three situations between different experiments as well as within a single recording period. The unique conditions of each experiment, including changes in one's bowel motility and ambient acoustic noise, can result in these variations. However, the device's capacity for potential utilization in capturing the characteristics of bowel sounds of different bowel diseases is still illustrated. These results serve as a reference that gives a foundation for further analysis and evaluation.

2.5 Automatic classification of bowel sounds by machine learning methods

In this subsection, we demostrate a simple application of this flexible device on the collection and classification of bowel sounds with BPNN. Previous studies have shown that the bowel sound is a useful physiological parameter reflecting information about bowel dysfunction, and the occurrence of other diseases such as diabetes mellitus [33]. Objective and quantitative evaluations of bowel sounds using spectral analyses or artificial neural networks aim at the diagnosis of the irritable bowel syndrome [9,13], Crohn's disease [13], intestinal obstruction [14], and acute abdominal diseases [15]. These findings focused on the pathophysiologic aspects of bowel disease, while other relevant factors, such as the type of ingested food, emotional state, or medications, were are not taken into consideration. In fact, the relationship between bowel sounds and types of ingested food remains unclear. As commonly known, intestinal health can be influenced by food components. It has been pointed out that an approximate doubling of total fiber intake from foods could reduce the risk of colorectal cancer by 40%, in populations with low-average intake of

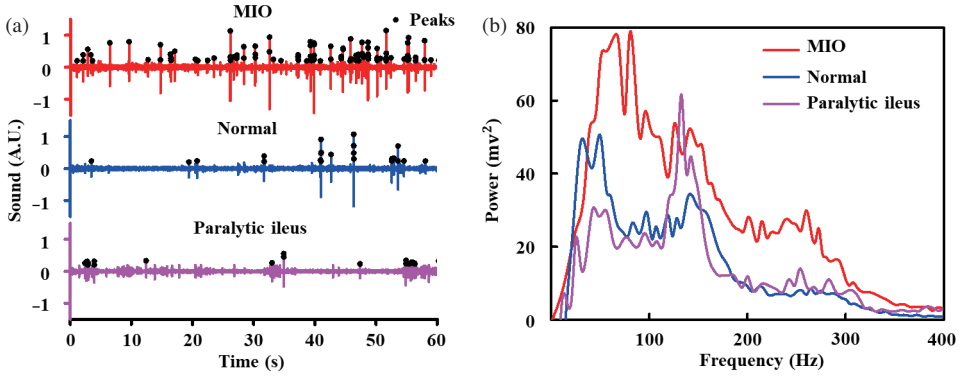

Figure 5 (Color online) Clinical tests of the device. (a) Typical waveform lines of bowel sounds from one normal subject (blue line) and two patients with MIO (red line) and paralytic ileus (pink line); (b) corresponding power envelope curves associated with the three studied cases.

dietary fiber [34]. Meanwhile, several recent studies have founded that diets with increased consumption of nuts may be associated with a significantly reduced cancer recurrence and death in patients with stage III colon cancer [35]. In this study, our device collected and classified bowel sounds produced in the digestion of different types of food, including nuts and oranges.

Sixteen healthy volunteers (12 males and 4 females, mean age±standard deviation: 26±3) participat in the study and are evenly divided into two groups. After fasting for twelve hours, people in two groups are asked to eat nuts and oranges at 8:00 am on the day of the study until they could not eat anymore. Bowel sound recordings, which span 3.5 h in toal, begin immediately after food intake in a silent room. The participants are allowed only an appropriate amount of water during the measurements. A total of 84 h of bowel sound recordings are obtained.

The processing step is described in Appendix C. Examples of FFT results of bowel sound segments at different times from four volunteers who ate nuts and oranges are shown in Figure 6(a). Frequency spectra acquired in different cases leads to their irregular power distributions. The distinction between these bowel sounds may result from density differences of contents in the small intestine, just as watermelon ripeness influences the sounds generated when knocking on the watermelon's outer surface.

Segmentation of bowel sound data results in 7875 bowel sound samples (3101 for nuts and 4774 for oranges). A K-fold cross-validation is implemented and the K is chosen as 10, which means that the total number of samples is randomly partitioned into ten equally sized groups. Of the ten groups, nine groups are used as training data, and the remaining group is used as the test set. The process is then repeated ten times with each group used once as a test set. Finally ten datasets are recognized by the BPNN algorithm (Figure 6(b)). The average of the overall recognition accuracy is 76.89% with a standard deviation of 3.29%. The algorithm's performance exceededs the results of the random classification. Accordingly, this serves as a proof-of-concept for the possible applications of the device, such as the evaluation of digestive function, recovery monitoring after operation, and auxiliary diagnosis of bowel problems. To achieve these goals, there is still a lot of room for improvement in problem analysis, extraction of features and the training process of modeling.

3 Conclusion

The concepts in the device and system provide a new way to non-invasively monitor and evaluate the bowel environment in real time. The integration of the 3D printed, flat, U-shaped elastomeric resonator and the ultra-soft shell realized a flexible and thin structure, and made the long-term use of our device possible. In addition, bowel sound activities were quantified based on conducted experiments at which the device was worn and recorded continuously for hours after food intake. For the evaluation of bowel sounds produced in the digestion of two types of food, the algorithm based on BPNN exhibited a good recognition accuracy for two bowel sounds. However, system improvements can be accomplished, including noise

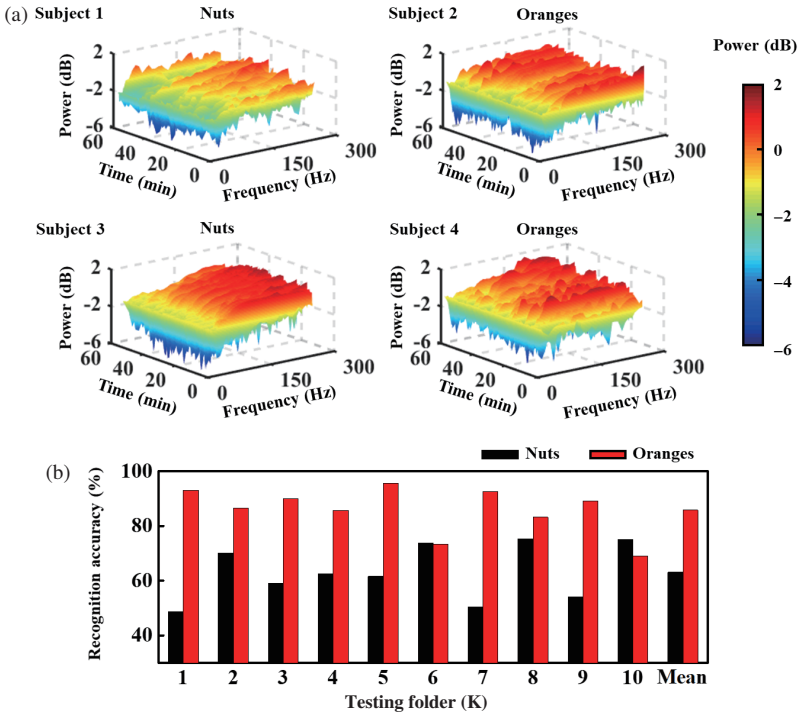

Figure 6 (Color online) Collecting and classification of bowel sounds. (a) FFT results of bowel sound segments at different times from four volunteers following the consumption of nuts and oranges; (b) recognition accuracy outcomes for two types of bowel sounds in the 10-fold cross-validation.

reduction, bending lifetime testing, and algorithmic research. Accordingly, it is necessary to carry out additional research to verify the feasibility of application of this system to more practical, clinical research paradigms.

4 Experimental section

Fabrication of the flexible acoustic device. The MEMS microphone chip (ADMP401, 3.76 mm×2.95 mm ×1.1 mm, analog device), the low power Bluetooth SoC (DA14580, Dialog), and other electronic components, are soldered on a commercial flexible printed circuit board (FPCB) with the use of surface mounted technology (SMT). The thin battery (13 mm×22 mm×0.5 mm) is obtained from Guangzhou Fullriver Battery New Technology. The elastomeric resonator, which is made of a multi-material composite (RWT-ENT-A40, 3D systems), is printed by a high-definition 3D printer (ProJet MJP 5600, 3D systems). It is then adhered to the FPCB by cyanoacrylate adhesive. The device and FPCB are placed into Ecoflex (00-30, Smooth-On) in a liquid state, and they are cured together in situ for 3 h.

Statistical and data analyses. Power envelope curves are obtained based on FFT and an envelope extraction process with used of OriginPro 9. These are shown in Figures 3 and 5. The value of the power envelope represents the mean-square amplitude (MSA):

$$\mathrm{MSA} = \frac{R^2 + I^2}{n^2},$$

where R and I are the real and imaginary parts of the FFT data, and n is the length of the input sequence. Only the upper envelope of MSA is detected and smoothed. The spectrogram shown in Figure 4 results from the application of FFT algorithm with a Hamming window filter and 12.5% overlap in MATLAB R2017a. As shown in Figure 6, the FFT results of each sound segment in the same test are put in one graph in chronological order by MATLAB R2017a. Other data graphs in this study are performed using OriginPro 9.

Mechanical modeling and FEA. FEA of sound intensity is performed with the use of a commercial software package (COMSOL Multiphysics 5.0). To simplify the simulation, only the cavity (air is the set material) of the 3D printed resonator is modeled with the free tetrahedral nodes, which allows the construction of an unstructured tetrahedral mesh. A hard sound boundary is added as a boundary condition.

Ethical approval for clinical tests One patient with MIO, one patient with paralytic ileus, and a healthy male, are recruited to participate in the clinical test, under the guidance and supervision of the staff members of the Peking Union Medical College Hospital. All procedures follow the guidelines of the International Review Board, and the conduct of the research study is approved by the Peking Union Medical College Hospital.

Acknowledgements This work was supported by National Basic Research Program of China (Grant No. 2015CB351900) and National Natural Science Foundation of China (Grant Nos. 11320101001, 11222220, 11625207).

References

1 Garner C G, Ehrenreich H. Non-invasive topographic analysis of intestinal activity in man on the basis of acustic phenomena. Res Exp Med, 1989, 189: 129–140
2 Harari D, Norton C, Lockwood L, et al. Treatment of constipation and fecal incontinence in stroke patients: randomized controlled trial. Stroke, 2004, 35: 2549–2555
3 Talley N J, Vakil N B, Moayyedi P. American gastroenterological association technical review on the evaluation of dyspepsia. Gastroenterology, 2005, 129: 1756–1780
4 Dagdeviren C, Javid F, Joe P, et al. Flexible piezoelectric devices for gastrointestinal motility sensing. Nat Biomed Eng, 2017, 1: 807–817
5 Inderjeeth A J, Webberley K M, Muir J, et al. The potential of computerised analysis of bowel sounds for diagnosis of gastrointestinal conditions: a systematic review. Syst Rev, 2018, 7: 124
6 Zhang Y, Jeon M, Rich L J, et al. Non-invasive multimodal functional imaging of the intestine with frozen micellar naphthalocyanines. Nat Nanotech, 2014, 9: 631–638
7 Kim K S, Seo J H, Song C G. Non-invasive algorithm for bowel motility estimation using a back-propagation neural network model of bowel sounds. Biomed Eng Online, 2011, 10: 69
8 Ching S S, Tan Y K. Spectral analysis of bowel sounds in intestinal obstruction using an electronic stethoscope. World J Gastroenterol, 2012, 18: 4585–4592
9 Craine B L, Silpa M, O'Toole C J. Computerized auscultation applied to irritable bowel syndrome. Digestive Dis Sci, 1999, 44: 1887–1892
10 Ranta R, Louis-Dorr V, Heinrich C, et al. Digestive activity evaluation by multichannel abdominal sounds analysis. IEEE Trans Biomed Eng, 2010, 57: 1507–1519
11 Baid H. A critical review of auscultating bowel sounds. British J Nursing, 2009, 18: 1125–1129
12 Feinberg A N, Feinberg L A, Atay O K. Gastrointestinal care of children and adolescents with developmental disabilities. Pediatr Clin North Am, 2008, 55: 1343–1358
13 Craine B L, Silpa M L, O'Toole C J. Enterotachogram analysis to distinguish irritable bowel syndrome from Crohn's disease. Digest Dis Sci, 2001, 46: 1974–1979
14 Yoshino H, Abe Y, Yoshino T, et al. Clinical application of spectral analysis of bowel sounds in intestinal obstruction. Dis Colon Rectum, 1990, 33: 753–757
15 Zaborski D, Halczak M, Grzesiak W, et al. Recording and analysis of bowel sounds. Euroasian J Hepatogastroenterology, 2015, 5: 67–73
16 Vasseur C, Devroede G, Dalle D, et al. Postprandial bowel sounds. IEEE Trans Biomed Eng, 1975, 22: 443–448
17 Drossman D A. The functional gastrointestinal disorders and the Rome II process. Gut, 1999, 45: 1–5
18 Holtmann G, Enck P. Stress and gastrointestinal motility in humans: a review of the literature. Neurogastroenterol Motil, 1991, 3: 245–254
19 Rekanos I T, Hadjileontiadis L J. An iterative kurtosis-based technique for the detection of nonstationary bioacoustic signals. Signal Process, 2006, 86: 3787–3795
20 Hadjileontiadis L J, Liatsos C N, Mavrogiannis C C, et al. Enhancement of bowel sounds by wavelet-based filtering. IEEE Trans Biomed Eng, 2000, 47: 876–886
21 Craine B L, Silpa M L, O'Toole C J. Two-dimensional positional mapping of gastrointestinal sounds in control and functional bowel syndrome patients. Digest Dis Sci, 2002, 47: 1290–1296
22 Gao W, Emaminejad S, Nyein H Y Y, et al. Fully integrated wearable sensor arrays for multiplexed in situ perspiration analysis. Nature, 2016, 529: 509–514
23 Gao G P, Hu B, Tian X L, et al. Experimental study of a wearable aperture-coupled patch antenna for wireless body area network. Microw Opt Technol Lett, 2017, 59: 761–766
24 Karthik V, Rao T R. SAR investigations on the exposure compliance of wearable wireless devices using infrared thermography. Bioelectromagnetics, 2018, 39: 451–459
25 Cai S S, Han Z Y, Wang F L, et al. Review on flexible photonics/electronics integrated devices and fabrication strategy. Sci China Inf Sci, 2018, 61: 060410
26 Chen S H, Pan T S, Yan Z C, et al. Flexible ultra-wideband rectangle monopole antenna with O-slot insertion design. Sci China Inf Sci, 2018, 61: 060414

27 Xu C Q, Liu Y, Yang Y T. An intelligent partitioning approach of the system-on-chip for flexible and stretchable systems. Sci China Inf Sci, 2018, 61: 060415
28 Mamun K A A, McFarlane N. Integrated real time bowel sound detector for artificial pancreas systems. Sens Bio-Sens Res, 2016, 7: 84–89
29 Zwikker C, Kosten C W. Sound Absorbing Materials. New York: Elsevier Publishing Company, Inc, 1949
30 Bies D A, Hansen C H. Engineering Noise Control: Theory and Practice. London: Spon Press, 2009
31 Fahy F J, Gardonio P. Sound and Structural Vibration: Radiation, Transmission and Response. Oxford: Academic Press, 2007
32 Georgoulis B. Bowel sounds. Proc R Soc Med, 1967, 60: 917–920
33 Yamaguchi K, Yamaguchi T, Odaka T, et al. Evaluation of gastrointestinal motility by computerized analysis of abdominal auscultation findings. J Gastroenterol Hepatol, 2006, 21: 510–514
34 Bingham S A, Day N E, Luben R, et al. Dietary fibre in food and protection against colorectal cancer in the European Prospective Investigation into Cancer and Nutrition (EPIC): an observational study. Lancet, 2003, 361: 1496–1501
35 Fadelu T, Zhang S, Niedzwiecki D, et al. Nut consumption and survival in patients with stage III Colon cancer: results from CALGB 89803 (Alliance). J Clin Oncol, 2018, 36: 1112–1120

Appendix A The calculation of f_r and f_0

The internal coincidence frequency f_0 of the gas in the pipe is defined by

$$f_0 = \frac{f_r}{4}\left(\frac{c_2}{343}\right),$$

where c_2 is the speed of sound inside the pipe and f_r is the ring frequency, which is

$$f_r = \frac{c_L}{2\pi a},$$

where c_L refers to the compressional wave speed in the pipe wall. In this way f_0 (approximately 20000 Hz) turns out to be much higher than the frequency of peak bowel sound, f_p (lower than 1000 Hz).

Appendix B Preprocessing of bowel sound data

Considering the difference of digestion rates for nuts and oranges, part of recordings of bowel sounds are cut out and only 90 min' recordings of each measurement are retained. For nuts and oranges, corresponding recordings in the first 30 min and 10 min respectively are cut out.

Firstly, the digital sound stream is filtered using a digital low-pass infinite impulse response (IIR) filter (0–600 Hz)[1)2)3)] for de-noising, to eliminate the possibilities of miscalculation for signals' features. Then sound signals are normalized to a scale of $[-1, 1]$ so that the amplitude of the signal is not affected by measurement sites and individual differences. After that, every bowel sound is extracted separately into 256-point segments (0.128 s). If the length of some certain sounds are larger than 256, then they are not considered in subsequent analysis. Besides, Hamming window is assigned to each individual segment.

After data segmentation, there are two types of features adopted for subsequent analysis: time-domain features and FFT results. In time domain, a single parameter is starting time, which is related to the time interval of occurrence of bowel sounds. For FFT results, the power of the frequency bands between 60 and 375 Hz is only chosen. Finally, each segment has 42 features.

1) Ranta R, Louis-Dorr V, Heinrich C, et al. Digestive activity evaluation by multichannel abdominal sounds analysis. IEEE Trans Biomed Eng, 2010, 57: 1507–1519.

2) Yoshino H, Abe Y, Yoshino T, et al. Clinical application of spectral analysis of bowel sounds in intestinal obstruction. Dis Colon Rectum, 1990, 33: 753–757.

3) Kim K-S, Seo J-H, Song C-G. Non-invasive algorithm for bowel motility estimation using a back-propagation neural network model of bowel sounds. Biomed Eng Online, 2011, 10: 69.